

Sucrose ester-based biocompatible microemulsions as vehicles for aceclofenac as a model drug: formulation approach using D-optimal mixture design

Marija N. Todosijević · Nebojša D. Cekić ·
Miroslav M. Savić · Mirjana Gašperlin ·
Danijela V. Randelović · Snežana D. Savić

Received: 10 April 2014 / Revised: 14 July 2014 / Accepted: 21 July 2014 / Published online: 5 August 2014
© Springer-Verlag Berlin Heidelberg 2014

Abstract We assessed the functionality of sucrose esters (sucrose laurate, myristate, palmitate, and stearate), relatively innocuous nonionic surfactants, in formulation of biocompatible microemulsions. The putative influence of surfactant structure on the extension of microemulsion region was explored through the construction of the pseudo-ternary phase diagrams for the isopropyl myristate/sucrose ester-isopropyl alcohol/water system, using the titration method and mixture experimental approach. Minor changes in surfactant tail length strongly affected the microemulsion area boundaries. D-optimal mixture design proved to be highly applicable in detecting the microemulsion regions. Examination of

conductivity, rheology, and thermal behavior of the selected sucrose laurate and sucrose myristate-based microemulsions, upon dilution with water, indicated existence of percolation threshold and suggested the phase inversion from water-in-oil to oil-in-water via a bicontinuous structure. Atomic force micrographs confirmed the suggested type of microemulsions and were valuable in further exploring their inner structure. The solubilization capacity of aceclofenac as a model drug has decreased as the water volume fraction in microemulsion increased. High surfactant concentration and the measured solubility of aceclofenac in microemulsion components suggested that the interfacial film may mostly contribute to aceclofenac solubilization.

Electronic supplementary material The online version of this article (doi:10.1007/s00396-014-3351-4) contains supplementary material, which is available to authorized users.

M. N. Todosijević · S. D. Savić (✉)
Department of Pharmaceutical Technology and Cosmetology,
Faculty of Pharmacy, University of Belgrade, Vojvode Stepe 450,
Belgrade 11221, Serbia
e-mail: snexs@pharmacy.bg.ac.rs

N. D. Cekić
Faculty of Technology, University of Niš, Leskovac 16000, Serbia

N. D. Cekić
DCP Hemigal, Leskovac 16000, Serbia

M. M. Savić
Department of Pharmacology, Faculty of Pharmacy, University of
Belgrade, Belgrade 11221, Serbia

M. Gašperlin
Department of Pharmaceutical Technology, Faculty of Pharmacy,
University of Ljubljana, 1000 Ljubljana, Slovenia

D. V. Randelović
ICTM—Institute of Microelectronic Technologies, University of
Belgrade, Belgrade 11000, Serbia

Keywords Biocompatible sucrose ester · Microemulsion ·
D-optimal mixture design · Atomic force microscopy ·
Aceclofenac

Introduction

Considerable attention for environmental protection and similarity with the structures of biological molecules have caused an increased interest of pharmaceutical industry toward sucrose esters (SEs) [1, 2]. They are natural, non-ionic tensides with low skin irritation potential and high environmental compatibility [3]. Available SEs are complex mixtures of mono-, di-, tri-, and polyesters of hydroxyl groups of sucrose (hydrophilic head) with different chain length fatty acid (lipophilic tail), which can be manufactured in wide range of hydrophilic–lipophilic balance (HLB) values [4, 5]. In addition, the proposed low skin sensitization potential and an established skin penetration enhancement have led to the increased research interest in the SEs' dermal/transdermal application,

particularly in advanced drug delivery systems [1]. Besides structure of the surfactant and physicochemical properties of the drug, the nature of the vehicle may also influence drug penetration following topical application. Thus, in order to improve the transport of a drug across the upper part of the skin, SE-based microemulsions may be taken into consideration. As thermodynamically stable, optically isotropic, transparent dispersions, microemulsions have a combination of features that make them highly effective in dermal/transdermal drug delivery, such as large surface area of the internal phase, improved drug solubility and long-term stability [6, 7]. Being potentially feasible in formulation of tailor-made drug delivery systems of satisfying safety profile, SEs are of interest to be explored in detail, as differences in their structure might lead them to behave differently at the oil–water interface and, consequently, affect the inner structure of microemulsions [8].

In contrast to the easy preparation, microemulsion characterization is more challenging and requires a multi-technique approach for fully understanding the relationship between microemulsion composition and their microstructure [9]. While freeze-fracture transmission electron microscopy is usually used as a valuable tool in visualization of inner microemulsion structuration, several major drawbacks of this technique have been reported [10–12]. We proposed that some of these artifacts and disadvantages, such as ice contamination, phase separation, and structural transition, might possibly be overcome by atomic force microscopy (AFM), a technique rarely employed for the evaluation of microemulsion structures [13] and used in the current study.

By affecting the localization of solubilized molecules, solubilization capacity of microemulsions strongly depends on their microstructure and physicochemical properties of the employed constituents [14]. Aceclofenac, a nonsteroidal anti-inflammatory drug, is indicated orally in the therapy of osteoarthritis, rheumatic arthritis, and ankylosing spondylitis [15]. Furthermore, characteristics such as low water solubility, short biological half-life, gastrointestinal adverse effects, and first-pass metabolism make aceclofenac an appropriate candidate for topical rather than oral application. Prospective transdermal delivery of aceclofenac loaded in microemulsions has several potential benefits such as improved drug solubility, increased patient compliance, as well as improvement of targeting. Hence, enhanced aceclofenac permeation could be useful in the therapy of inflammatory and painful states of bones, ligaments, joints, tendons, and muscles [16, 17].

To summarize, the first aim of the present research was to evaluate the effect of the surfactant tail length on the phase behavior and SEs' potential to form microemulsions using pseudo-ternary phase diagrams. However, phase diagram construction requires numerous time-consuming

and repetitive experiments, and therefore, the second goal of the study was to investigate the usefulness of D-optimal mixture design as an alternative approach to determine the microemulsion area in a more effective way. Bearing in mind that structure of microemulsions might have deep influence on the release rate as well as percutaneous penetration of the solubilized drug [14, 18, 19], the further aim of the study was to evaluate the types of microemulsions obtainable during dilution with water, using several techniques such as conductivity, viscosity, differential scanning calorimetry (DSC), and AFM. Finally, in order to formulate an optimized vehicle for aceclofenac dermal/transdermal delivery with minimum content of surfactant and cosurfactant, solubilization studies with this drug have been performed.

Materials and methods

Materials

Aceclofenac was obtained by Jinan Jiaquan Chemical Co. Ltd, China. SEs (sucrose laurate D-1216, sucrose myristate C-1416, sucrose palmitate D-1616, and sucrose stearate D-1816) were a generous gift by Mitsubishi-Kagaku Foods Corporation (Tokyo, Japan). Isopropyl myristate (IPM) was purchased from Comcen (Belgrade, Serbia). Isopropyl alcohol (IPA) was obtained from Brenntag (Wien, Austria). All of the components were of pharmaceutical grade and used as received, without further purification. Ultra-purified water (W), used in this research, was obtained with a GenPure apparatus (TKA Wasseranfertigungssysteme GmbH, Neidelerbert, Germany).

Construction of pseudo-ternary phase diagrams

Four different surfactants, namely sucrose laurate (SL), sucrose myristate (SM), sucrose palmitate (SP), and sucrose stearate (SS), with the same head group but differ in their tail length were chosen for screening on the basis of their emulsification efficiency, i.e., capability to form a large microemulsion area. It should be emphasized that SEs with the same HLB value of 16 were chosen. The phase behavior of systems consisting of oil, surfactant blend (treated as a pseudo-component), and water was evaluated by titration method at room temperature. IPM was used as an oil phase, while surfactant blend consisted of the main surfactant (SL, SM, SP, or SS) and cosurfactant IPA in the weight ratio 1:1 (K_m). Firstly, a precise amount of each SE was mixed with the required amount of IPA (K_m ratio 1:1) under magnetic stirring, and this ratio was kept constant throughout phase behavior investigation. Mixtures of oil and surfactant blend were combined in different surfactant + cosurfactant-to-oil weight ratios

(SCoS/O), from 9:1 to 1:9 (*w/w*), and subsequently slowly titrated drop by drop with water until the respective solubilization limit was reached. Samples were left for equilibration for 15 min between each addition of water aliquot. After vigorous vortexing, only homogenous, single-phase, low viscous mixtures were classified as microemulsions based on their transparency and optical isotropy checked visually and by using optical methods. Boundaries of microemulsion region were defined by determination of the percent of water incorporated when the previously transparent, isotropic systems became cloudy or turbid.

Evaluation of SEs solubility in the oil and water phase

In order to better understand the influence of the SEs on the phase behavior as well as on the boundaries of microemulsion area, a solubility study of SEs in the oil and the water phase was performed by shake flask method using IKA® KS 260 basic (IKA® Werke GmbH & Company KG Staufen, Germany) shaker. An excess amount of SEs was added to 5 ml of both, IPM and ultra-purified water, in Erlenmeyer flasks, which were then shaken at 300 rpm for 48 h. After centrifugation of the samples at 3,000 min⁻¹ for 30 min (Centrifuge MPW-56, MPW Med. Instruments, Warszawa, Poland), an aliquot of the supernatant was properly diluted with methanol, and concentration of SEs was determined using spectrophotometer (Varian Cary-100 UV–VIS Varian BV, Middelburg, Netherlands) at 210 nm. Experiments were performed in triplicate, at room temperature.

Formulation selection based on the phase diagrams and preparation of samples

From each of the constructed phase diagrams, formulations were chosen along dilution line, with maximum water solubilization capacity drawn to the opposite water side of the phase diagram. Microemulsion vehicles, which differ in the water volume fraction (Φ_w), were prepared for further characterization, by adding an appropriate mass of water into mixture of oil and surfactant blend (K_m ratio 1:1) under magnetic stirring. The samples were filled into 20-ml headspace glass vials with crimp cups and left for 48 h to equilibrate before further characterization.

Polarization microscopy

Optical isotropy of microemulsions was evaluated using Motic digital microscope DMB3-223ASC and Motic Images Plus v.2.0 software (Motic GmbH, Wetzlar, Germany). Samples prepared during the construction of the pseudo-ternary phase diagrams as well as samples prepared for further characterization were checked for the lack of birefringence. In case of microemulsions, the field of view remains dark, as

transparent, isotropic systems, such as microemulsions, do not interfere with the polarized light [7, 20].

Spectroscopic characterization of optical clarity

Microemulsions as macroscopically homogenous and transparent systems exhibit good optical transparency in the visible range (500–760 nm) [21]. Therefore, besides using polarization microscopy, optical clarity of microemulsions was checked spectroscopically (Varian Cary 100 UV–VIS spectrophotometer; Varian BV, Middelburg, Netherlands) by measuring transmittance of samples at 700 nm, using ultra-purified water as blank.

Mixture experimental design and statistical analysis

In the present study, D-optimal mixture design was specifically selected because three factors can be evaluated by varying their concentrations simultaneously and keeping their total amount constant, which is necessary for construction of pseudo-ternary phase diagrams. Thus, quantities of microemulsion components (factors) cannot be changed independently, since they are all part of a formulation and their percent amounts sum up to 100 %. However, the measured response is assumed to be functionally related to the component weight fraction and not depend on the total amount of the mixture [22]. Additionally, D-optimal design minimizes the variance associated with the estimates of specified model coefficients [23]. Design Expert® (version 7.0.0, Stat-Ease, Inc., Minneapolis, MN, USA) was used to generate D-optimal mixture design in order to predict boundaries of microemulsion area, for each of investigated systems.

Definition of the constraints and the factors tested

D-optimal mixture experimental study was designed based on a three-component system: the surfactant blend (SE/IPA, K_m ratio 1:1)—factor *A*, oil phase (IPM)—factor *B*, and water phase—factor *C*. Bound restrictions on the component proportions (X_i) are necessary in D-optimal mixture design, in order to limit the feasible space of variables between the lower and upper constraints. The general form of the constrained mixture problem is as follows:

$$L_i \leq X_i \leq H_i$$

where L_i and H_i denote lower and upper bounds for the X_i -th component, respectively [22, 24].

Thus, selection of the constraints deserves particular attention, as the candidate points, and consequently the chosen experimental region, must be representative in order to achieve an adequate coverage of the pseudo-ternary phase

diagrams. In the present study, constraints for the percent amounts of components were set on the basis of our pilot studies and the corresponding subject matter knowledge:

$$\begin{aligned} 10\% &\leq A(\text{SE : IPA}, K_m \text{ ratio } 1 : 1) \leq 90\% \\ 5\% &\leq B(\text{IPM}) \leq 45\% \\ 5\% &\leq C(\text{W}) \leq 45\% \\ A + B + C &= 100\% \end{aligned} \quad (1)$$

On the basis of the D-optimal mixture model, experimental design consisted of total 19 experimental runs in randomly arranged order to avoid any systematic bias in the outcomes. The design consisted of the following candidate points: four vertices, four centers of edges, an overall center point, and four interior points of the constrained region. The obtained design mixture space presented in Fig. 1, with a rhomboidal shape, is defined by the low and high level constraints on each factor. Each corner of the equilateral triangle corresponds to the upper bond appointed for each factor.

To simplify computations, the components A , B , and C were transformed into pseudo-components. This transformation is useful since it may provide more accurate estimation of model coefficients in comparison with using the original component system [25]. The following equation was used for conversion of percent amount (% w/w) of components into L-pseudo-components (the minimum value of each component becomes 0 as the maximum value approaches 1):

$$\text{Pseudo} = \frac{(\text{Real} - L_i)}{1 - \sum L_i} \quad (2)$$

where L_i is the lower constraint and $\sum L_i$ is the sum of all lower constraints in terms of real value [23]. Real components are defined as follows:

$$\text{Real} = \frac{A_i}{\sum A_i} \quad (3)$$

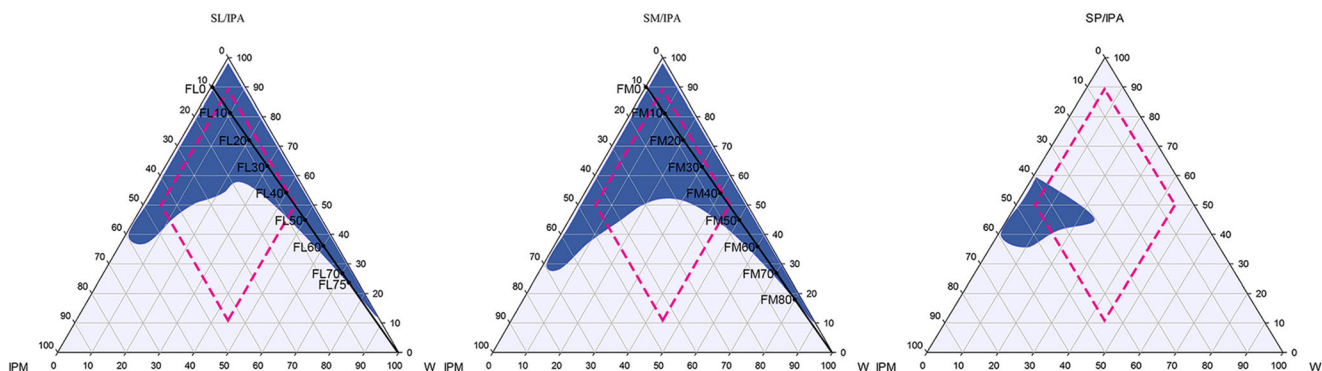


Fig. 1 Pseudo-ternary phase diagrams of microemulsion composed of isopropyl myristate/sucrose ester-isopropyl alcohol/water using as a sucrose ester: sucrose laurate, sucrose myristate, and sucrose palmitate, respectively, at K_m ratio 1:1. The *selected line* represents water dilution

where A_i is the percent amount (% w/w) of each component and $\sum A_i$ is the sum of component amounts.

Microemulsion transmittance percentage ($T(\%)/100$) at 700 nm, which suggests the lack of macroscopic phase separation, was chosen as the dependent variable to be maximized (response). $T(\%)/100$ values higher than 0.99 were set as the regions of stable microemulsions [26]. This parameter, measured with UV/VIS spectrophotometer, indicated optical clarity and transparency of microemulsions.

Statistical analysis

Statistical analysis was performed using the Design Expert® software. All the responses were simultaneously fitted to the mathematical models, and the adequacy of the polynomial equations was verified by comparisons of several statistical parameters, including the multiple correlation coefficients (R^2) as well as the adjusted multiple correlation coefficients (adjusted R^2) (both of them should be as higher as possible), adequate precision (ratio greater than 4 is desirable), predicted residual error sum of squares (PRESS; it should be small for the best model since it indicates how well the model fits the data), and F value provided by analysis of variance (ANOVA).

Characterization

Electrical conductivity measurements

To enable electrical conductivity of the nonionic microemulsions, a small amount of an aqueous electrolyte could be added in the system [27]. Thus, instead of ultra-purified water, an aqueous solution of 0.01 M NaCl was used in the preparation of microemulsions. Changes in electrical conductivity values (σ) of microemulsions with gradual addition of 0.01 M NaCl aqueous solution, allowing time for attainment of the equilibrium, were examined with CDM23

conductivity meter (Radiometer, Copenhagen, Denmark). A precise amount of an aqueous solution of NaCl was continuously added into the initial mixture with SCoS/O of 9:1. The measurements were carried out in triplicate at 25 ± 1 °C.

Rheological measurements

The rheological behavior of the prepared samples was evaluated using DV-III ULTRA Programmable Rheometer and Rheocalc software v.4.3 (Brookfield Engineering Laboratories, Middlesboro USA), coupled with cone and plate measuring device at 20 ± 1 °C. The shear stress measurements were carried out within the shear rate range from 75 to 750 s^{-1} and vice versa for up and down curves, respectively, and the flow curves were evaluated by fitting the experimental data to Newtonian, Bingham, and Ostwald model. For the examination of the relationship between water concentration in microemulsions and viscosity, the apparent viscosity values (η) at the shear rate of 300 s^{-1} were used.

Differential scanning calorimetry

To investigate the internal structure and type of prepared microemulsions, DSC measurements were performed in a cooling mode with a Mettler Toledo DSC 1, STAR^c System (Mettler Toledo GmbH Analytical, Giessen, Germany). Approximately 5 to 10 mg of microemulsion samples were precisely weighted in a small aluminum pans and immediately hermetically sealed by a mechanical press. An empty hermetically closed aluminum pan was used as a reference. Samples were cooled from 25 to -60 °C at a cooling rate of 5 °C/min, under constant nitrogen flow (50 ml/min). To examine thermoanalytical parameters, such as enthalpy, onset, and peak temperature, the area of the relevant DSC peak was integrated, using Mettler Toledo STAR^c Software.

Atomic force microscopy (AFM)

AFM measurements were performed with NTEGRA prima atomic force microscope (NT-MDT, Moscow, Russia). As sample preparation can potentially introduce artifacts, a drop (10 μL) of the sample was directly deposited onto a small, circular mica disc (Highest Grade V1 AFM Mica Discs; Ted Pella Inc., Redding, California) and dried in desiccator or in vacuum to remove excess water, in order to find optimum preparation method.

Due to the consistency of the samples, measurements were carried out in air using an intermittent contact AFM mode and NT-MDT NSGO1 silicon cantilevers (N-type, Antimony doped, Au reflective coating). Parameters of used cantilevers were set as follows: nominal force constant 5.1 N/m, resonance frequency 87–230 kHz, driving frequency 148 kHz, and line scanning frequency 1 Hz. For the investigated

samples, both topography and “error signal” AFM images were taken and later analyzed using the software Image Analysis 2.2.0 (NT-MDT, Moscow, Russia).

Solubilization evaluation of pharmaceutical active ingredient—aceclofenac

In order to decrease the amount of both, surfactant and cosurfactant, determination of solubilization capacity of numerous microemulsions along the selected dilution line was carried out. Aceclofenac was added to the readily prepared microemulsions to give 2 % (w/w) concentration of drug and mixed under magnetic stirring at room temperature. The samples were filled into 20-ml headspace glass vials with crimp cups and stored at room temperature for 48 h. Microemulsions with sufficient solubilization capacity for aceclofenac were identified based on their visual appearance and optical behavior using polarization microscopy, as transparent, monophasic systems without any physical change (e.g., undissolved drug particles, blurriness).

Evaluation of aceclofenac solubility in the liquid excipients

Aceclofenac solubility in the oil phase, water phase, and cosurfactant and surfactant blends (K_m ratio 1:1) was evaluated by shake flask method using IKA[®] KS 260 basic (IKA[®] Werke GmbH & Company KG Staufen, Germany) shaker. An excess amount of the drug was added to 5 ml of each sample in Erlenmeyer flasks, and the resulting mixtures were continuously shaken for 48 h, at mixing rate of 300 rpm. After that, in order to remove undissolved drug, the samples were centrifuged at $3,000 \text{ min}^{-1}$ for 30 min (Centrifuge MPW-56, MPW Med. Instruments, Warszawa, Poland). The supernatant was separated and filtered through 0.22- μm membrane filter. Concentration of aceclofenac in the supernatant was determined spectroscopically, after proper dilution with methanol, at 274 nm (Varian Cary-100 UV-VIS spectrophotometer; Varian BV, Middelburg, Netherlands). Experiments were performed in triplicate, at room temperature.

Results and discussion

Pseudo-ternary phase diagrams and surfactant chain length effect on the microemulsion formation

SS was not miscible in IPA at the used experimental conditions; thus, Fig. 1 represents three pseudo-ternary phase diagrams of quaternary systems IPM/SE-IPA/W (K_m ratio 1:1) determined at room temperature. As SEs on their own are incapable to reduce the interfacial tension to the extent that allows the formation of microemulsion [28], IPA was

introduced as a cosurfactant. By interaction with the surfactant molecules, the presence of IPA in the interfacial region strongly influences their packing, leading to an increased interfacial flexibility (or fluidity) and imparting an optimized curvature necessary for spontaneous microemulsion formation [9, 29]. Considering the same HLB value of SEs, a similar reduction in the interfacial tension between the water and the oil phase in the microemulsion system is expected. Thus, an evident difference among the presented phase diagrams, in spite of the same HLB value, suggests that chemical structure of the surfactant as well as chain stiffness profoundly affected the phase behavior of IPM/SE-IPA/W mixtures, probably by influencing the packing of surfactant molecules at the oil–water interface. However, the SP-based microemulsions existed in an extremely narrow area, while the observed water solubilization capacity in the presence of SL and SM was much greater. The apparent increase of microemulsion region in SL- and SM-based systems may be ascribed to formation of an interfacial film that is less sensitive to water dilution, when compared to SP. Such approach is in line with the report that emulsion capacity of the surfactants decreases as the hydrocarbon chain length increases [30]. Due to the fact that SEs have the same head group but differ in their tail length, the head group steric repulsions for this homologous family of molecules should not affect the size of microemulsion area [31]. Accordingly, a long chain surfactant makes the interface more rigid, limiting its flexibility, and hence a surfactant with short chain length should be able to bind more water compared to the surfactant with a longer tail. This might suggest that increasing carbon number of the chain leads to the disruption of the packing of the surfactants at the oil–water interface. Notably, the present results follow the observation that increasing SE chain length will decrease the total monophasic area [32]. In addition, these results could be further explained with the obtained values of SE solubility in ultra-purified water and IPM. As given in Supplementary Material Table 1, solubility of SP in ultra-purified water was almost ten times lower than solubility of both SL and SM, while the observed solubility values of all SEs in IPM were comparable. As expected, solubility in water phase decreased with alkyl tail length increase. Thus, reduction in the total monophasic region, together with existence of microemulsion area in the oil-rich region in case of SP, may be a consequence of the lower solubility of SP in the water phase, which surely plays an important role in governing the amount of solubilized water. Thus, SL and SM were able to bind more water due to their shorter chain length and higher water solubility compared to SP. Such results highlight the importance of assessing in parallel the HLB value and structure, as well as solubility of surfactants in components of a microemulsion system.

Interestingly, comparing the influence of the tail length of SL and SM, the slightly higher effectiveness and consequently

wider microemulsion area were observed in the system prepared with SM as surfactant, perhaps because of greater oil molecule penetration into the hydrophobic region of the surfactant film. It has earlier been reported that compatibility of the hydrophobic part of surfactant and oil seems to be an important parameter that affects their mutual miscibility and therefore the oil penetration into the surfactant film, influencing the total microemulsion area [30, 32]. Despite lower solubility in water phase in comparison to SL, the same chain length of SM and IPM enables incorporating of IPM, as small volume oil, into the interfacial film which results in increasing interfacial flexibility and reduction of the interfacial tension and therefore extent of incorporated water. As expected, the highest water incorporation was achieved at SCoS/O of 9:1 where systems remained optically clear, isotropic, low viscous liquids up to an added Φ_w of 77.78 and 80.62 % (w/w) in case of SL and SM, respectively. Thus, microemulsion samples prepared along this dilution line were used for further structural characterization (Fig. 1).

D-optimal mixture design

There is a growing interest for *in silico* techniques for prediction of the phase behavior of microemulsion systems. The artificial neural networks (ANNs) are powerful data modeling tools utilized in several studies with the aim to evaluate boundaries of microemulsion systems [33–35]. The building process of ANN model can last for a long time, since it requires the choice of the network type suitable for the studied problem, the establishment of the network architecture (the number of layers and the number of neurons in the hidden layer(s)), selection of network activation function, training algorithm, and parameters specific for the training algorithm. Additionally, development of an ANN model with high generalization ability usually requires a greater number of data compared to mixture experimental approach, as the data set is divided into training, test, and validation subsets. Since ANN cannot provide a mathematical model giving quantitative relationship between the inputs and outputs and does not provide any information regarding statistical significance of the effects of investigated factors and their interaction, it is often considered as the black box models. On the other hand, the main outcome in D-optimal mixture design is the mathematical model which quantitatively describes relation between factors, together with the corresponding statistical analysis [36, 37].

Taking into account all the above reasons, we considered D-optimal mixture design as a suitable, time-saving, and economical *in silico* technique for the purpose of our study. D-optimal mixture design was used in order to rapidly obtain microemulsion boundaries for the three investigated systems and to confirm the experimentally obtained pseudo-ternary phase diagrams. Table 1 summarizes the conditions of the 19

Table 1 The 19 sets of run conditions determined by D-optimal mixture design and corresponding experimental response values

Formulation	Real components			L-pseudo-components			Responses		
	A-SE/IPA [% w/w]	B-IPM [% w/w]	C-W [% w/w]	A-SE/IPA	B-IPM	C-W	T(%) / 100 (SL)	T(%) / 100 (SM)	T(%) / 100 (SP)
F1	30	45	25	0.250	0.500	0.250	0.005123	0.005793	0.006401
F2	50	45	5	0.500	0.500	0.000	1	1	1
F3	50	15	35	0.500	0.125	0.375	0.010604	0.999599	1
F4	90	5	5	1.000	0.000	0.000	1	0.991789	0.000424
F5	30	25	45	0.250	0.250	0.500	0.001178	0.009150	0.001788
F6	10	45	45	0.000	0.500	0.500	0.000158	0.000272	0.000171
F7	70	5	25	0.750	0.000	0.250	1	0.995627	0.002454
F8	50	25	25	0.500	0.250	0.250	0.009034	1	1
F9	30	35	35	0.250	0.375	0.375	0.001670	0.002507	0.005453
F10	50	35	15	0.500	0.375	0.125	1	1	1
F11	50	45	5	0.500	0.500	0.000	1	1	1
F12	10	45	45	0.000	0.500	0.500	0.000163	0.000273	0.000180
F13	50	5	45	0.500	0.000	0.500	1	0.996189	0.017210
F14	90	5	5	1.000	0.000	0.000	1	0.991796	0.000571
F15	70	15	15	0.750	0.125	0.125	1	1	0.026441
F16	30	45	25	0.250	0.500	0.250	0.004008	0.006123	0.005213
F17	50	5	45	0.500	0.000	0.500	1	0.996108	0.018240
F18	30	25	45	0.250	0.250	0.500	0.001270	0.000985	0.001700
F19	70	25	5	0.750	0.250	0.000	1	1	0.037024

experimental runs and the corresponding observations for the response.

As already shown by Furlanetto et al. [25], modeling of $T(\%)$ may be challenging due to high range of responses (from almost 0 to 100 %). In principle, when responses vary over several orders of magnitude (response range greater than 10), a transformation is required. In this case, logit transformation is a useful tool if the response has a finite range from 0 to 100 %, since it spreads out the values near the boundaries [23]. Consequently, logit transformation was used as it was required to improve the model. In addition, as a part of the experimental design, five replicates of test formulations were measured and they agreed well to each other, indicating a good reproducibility of sample preparations and analytical techniques.

For SL-based system, the modified cubic model showed superior fit as the R^2 and adjusted R^2 values (0.9775 and 0.9595, respectively) were the highest, PRESS value was the lowest (94.92), adequate precision equaled 16.493, and p value was less than 0.0001, indicating the statistical significance of the model. In addition, the observed responses showed that best-fitted model for SM-based system was special cubic model due to p value < 0.0001, the highest R^2 and adjusted R^2 values (0.8996 and 0.8494, respectively), the lowest PRESS value (355.81), and adequate precision greater than 4 (13.793). In spite of

relatively small value of R^2 and adjusted R^2 (0.5785 and 0.4581, respectively) for SP-based systems, the signal-to-noise ratio was found to be 6.812, indicating an adequate signal and implies the adequacy of the model used to navigate the design space. The p value for the modified quadratic model was less than 0.05, and no significant improvement was achieved by adding special cubic term. Therefore, the refined polynomial equations where only significant model terms were included, which best describe the relationship between $T(\%)/100$ and microemulsion components, can be written as follows for SL, SM and SP-based systems, respectively:

$$\begin{aligned} \text{Logit}\left(\frac{T(\%)}{100}\right) &= \text{Ln}\left(\frac{T(\%)/100}{1-T(\%)/100}\right) = 14.06A - 222.58B \\ &+ 348.90C + 472.32AB - 670.66AC - 286.72BC \\ &- 312.61AB(A-B) + 449.38AC(A-C) + 782.99BC(B-C) \end{aligned} \quad (4)$$

$$\begin{aligned} \text{Logit}\left(\frac{T(\%)}{100}\right) &= \text{Ln}\left(\frac{T(\%)/100}{1-T(\%)/100}\right) = 3.74A - 58.17B \\ &- 45.31C + 162.34AB + 101.54AC + 168.81BC \\ &- 376.11ABC \end{aligned} \quad (5)$$

$$\text{Logit}\left(\frac{T(\%)}{100}\right) = \text{Ln}\left(\frac{T(\%)/100}{1-T(\%)/100}\right)$$

$$= -9.11A - 8.57B - 16.41C + 78.22AB + 41.37AC \quad (6)$$

A positive value in polynomial equation indicates synergistic effect of the factor on the response, while negative value indicates an inverse relationship between the factor and the response. As the coefficient is larger, the expected influence on the response is stronger and vice versa [26]. Equations 4–6 can be additionally used to calculate the predicted values for other formulations in design space.

Eventually, 2D contour plots and 3D surface plots of the $T(\%)/100$ across the selected factors were constructed, using the selected regression models, to further elucidate the relationship between the constituent weight fractions and the corresponding microemulsion area, as shown in Fig. 2. The 2D plots are shown in the form of pseudo-ternary diagrams in which $T(\%)/100$ at each composition is represented by the contour lines. However, when all the components are simultaneously changed, only the 3D surface plot of the model is able to clearly show the effect of the independent variables on the responses of dependent variables [24]. Finally, it can be inferred that regions with predicted $T(\%)/100$ values greater than 0.99 (marked with red in Fig. 2) and microemulsion regions identified via classical approach (shown in Fig. 1) are in a very good agreement. Thus, these observations highly support the usage of D-optimal mixture design where rapid

observation of microemulsion boundaries should be of paramount significance.

Characterization of colloidal structure

Electrical conductivity measurements

The relationship between Φ_w and σ of the investigated systems is presented in Fig. 3. It is evident that σ exhibited a continuously increasing trend as Φ_w increased. The obtained plots of σ versus Φ_w fit to a 2° polynomial equation with satisfying correlation coefficients, as given below for SL- and SM-based microemulsions, respectively:

$$\sigma = 1357.4\Phi_w^2 + 50.533\Phi_w - 4.8776 \quad (7)$$

$$R^2 = 0.9997$$

$$\sigma = 1430.5\Phi_w^2 - 16.676\Phi_w - 2.3633 \quad (8)$$

$$R^2 = 0.9998$$

In both SL- and SM-based systems, σ increased with increasing Φ_w , and this similar behavior may be explained by the same localization of SL and SM at the oil–water interface. The existence of three different slopes on conductivity profiles, as given in Supplementary Material Fig. 1, may be associated with three regions that differ in the inner microstructure. Similar dependence of the σ on Φ_w in

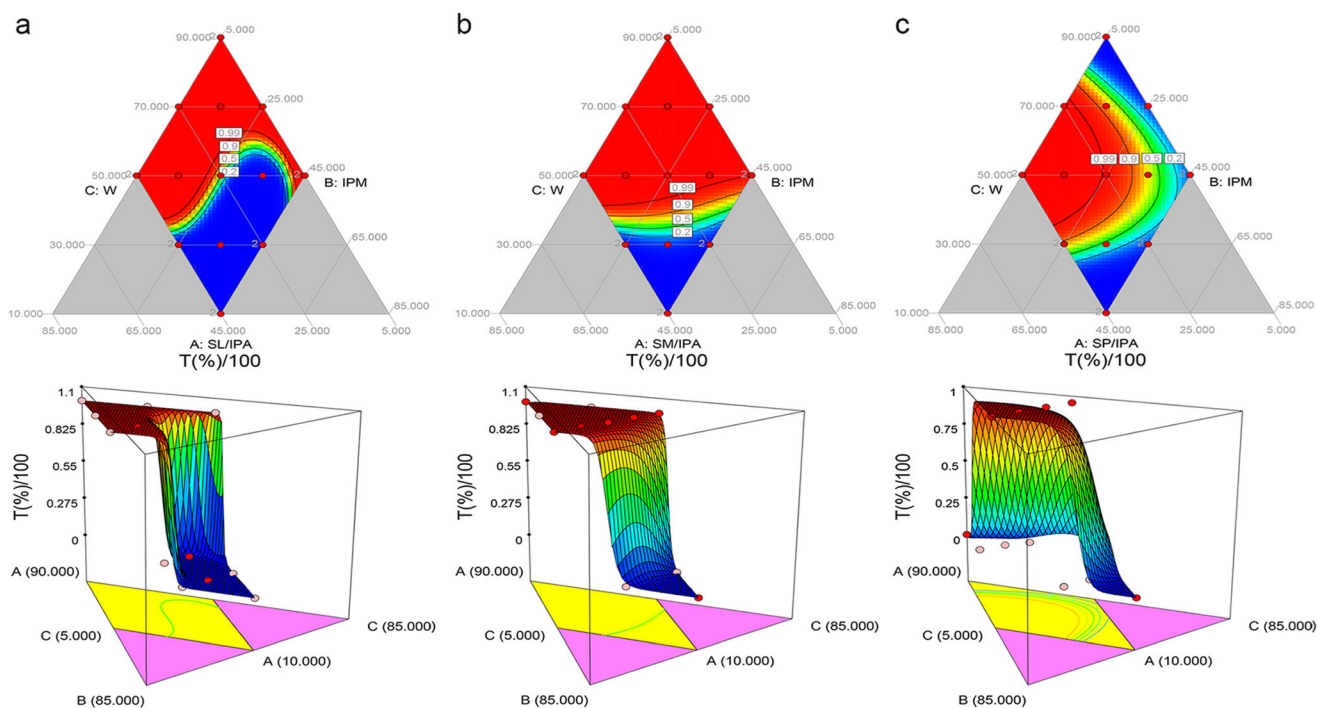


Fig. 2 2D contour plots and corresponding 3D surface plots illustrating the effect of the mixture composition on $T(\%)/100$ for IPM/SE-IPA/W system, where SE corresponds to SL, SM, and SP, respectively

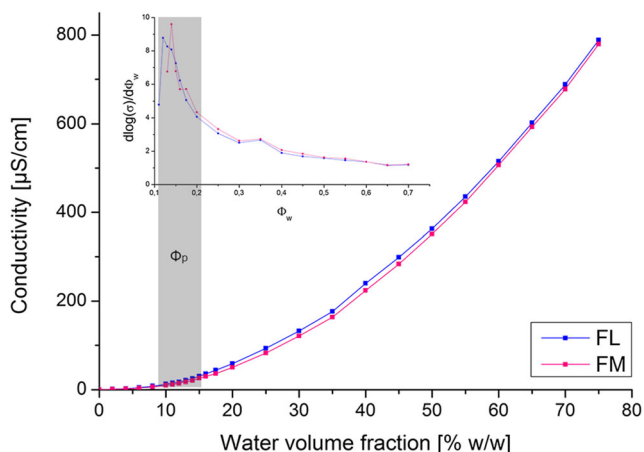


Fig. 3 Electrical conductivity (σ) as a function of the water volume fraction (Φ_w) for the IPM/SL-IPA/W (FL) and IPM/SM-IPA/W (FM) microemulsions at SCoS/O ratio 9:1. Selected gray region corresponds to the percolation threshold (Φ_p). Inset: The first derivative of logarithm of σ

microemulsion systems, after addition of salt, was reported elsewhere [14, 38]. However, three theories have been proposed as explanation of the aforementioned structural transition: an abrupt inversion, a phase separation, and gradual changes through bicontinuous structures (known as “percolation theory”) [39]. Since the investigated systems with SL and SM as surfactants remained isotropic during water titration, the percolation theory explanation was pursued in our research.

It must be emphasized that practically negligible σ values, less than 10 $\mu\text{S/cm}$, obtained for microemulsions with low Φ_w , suggest dispersions of noninteracted water droplets surrounded by an insulating surfactant film that prevents water from conducting. These results are in accordance with previous observations related to the conductance of spherical type microemulsions, suggesting existence of water-in-oil (W/O) microemulsions in which water globules are dispersed in nonconducting oil phase and hence contribute little to the σ of systems [10, 27, 29]. Initial increase of σ possibly occurs due to progressive hydration of the hydrophilic head group of SEs. When Φ_w reaches and exceeds a critical value for sharp linear enhancement of σ , an attractive interaction between discrete water droplets may become stronger leading to their collision. Actually, droplets’ interface becomes fluid enough to coalesce during collisions, resulting in the formation of clusters and water channels responsible for increased σ [20, 40]. As dynamic systems, the clusters constantly reorganize due to Brownian motion. This behavior can be explained with the aid of percolation theory, where interactions between water globules as well as their clustering play a crucial role [19, 29, 38, 40]. In fact, it may be seen that σ increases slightly up to critical Φ_w known as percolation threshold volume fraction (Φ_p), followed by a steep increase due to partial water drift to the outer phase and thus transition from an oil-continuous to bicontinuous microemulsions may take place.

Sharp growth in σ has widely been considered as the most important characteristic of a percolation concept; therefore, Φ_p is most accurately obtained from the conductivity data [39]. Thus, variation in σ (i.e., the profile of the plot of σ against Φ_w) can be interpreted by two separate asymptotic scaling power laws as given below:

$$\sigma = A(\Phi_p - \Phi_w)^{-s} (\Phi_w < \Phi_p) \quad (9)$$

$$\sigma = B(\Phi_w - \Phi_p)^t (\Phi_w > \Phi_p) \quad (10)$$

with exponents that are different above and below the percolation threshold [30, 41]. In this *power scaling approach* A and B are free parameters, while s and t are constants in the range 0.5–1.2 and 1.2–2.1, respectively, which depend on the dimensionality of the percolating system (i.e., number of variables) and not on the details of the geometric structures or interactions. When Φ_w is greater than Φ_p , σ obeys Eq. 10. The above equations are only valid near Φ_p and cannot be extrapolated to infinite dilution. Another reported drawback suggests that these equations are not applicable to the immediate vicinity of Φ_p , as continuous variation occurs within narrow interval around percolation threshold [10, 38, 40].

Alternatively, providing that a distinct difference in the area above and below the curve exists, the percolation threshold could be best determined from the first derivative $d\log(\sigma)/d\Phi_w$ as a function of Φ_w [10, 19, 32]. Actually, the value predicted by *first derivative approach* was more in agreement with the point of inflection noted in the plot of viscosity against Φ_w than that predicted by the power scaling method. Thus, for each data, quantity $d\log(\sigma)/d\Phi_w$ was evaluated. This quantity is sharply peaked and maximum of plot $d\log(\sigma)/d\Phi_w$ versus Φ_w confirms the presence of percolative behavior and coincides well with the percolation threshold [38, 42, 43]. Therefore, the obtained Φ_p values were 12 and 14 %, for systems IPM/SL-IPA/W and IPM/SM-IPA/W, respectively, as presented in Fig. 3 (inset). Our results suggested that with increasing surfactant chain length, the value of percolation threshold increases, corresponding to the stronger attractive inter-droplet interaction in case of W/SL-IPA/IPM system. This behavior can be explained as follows: the interfacial monolayer in these systems is made up of alcohols and surfactants, having their polar groups in contact with the water, and their alkyl chains in contact with the oil. Attraction between droplets depends on the interpenetration of the interfacial layers that brings the water cores close enough [30]. Thus, the different alkyl chain length is responsible for the higher degree of the overlapping in case of SL.

As Φ_w further increases, the number of the proposed clusters above percolation threshold also increases, causing rapid raise in σ . The second change in slope (Supplementary Material Fig. 1) probably occurs due to a complete transition

from bicontinuous structure to dispersion of oil droplets in the continuous water phase. The very high values of σ at high Φ_w in both systems may be ascribed to the presence of NaCl ions in the external water phase. At this point, head groups of SEs are exposed to the continuous phase and become saturated with water, leading to the maximum conductivity values.

Rheological measurements

Dependence of linear shear stress (τ), as well as independence of η on shear rate ($\dot{\gamma}$), indicates that all microemulsions have Newtonian flow behavior without thixotropy, as presented in Fig. 4a, b. These results follow the earlier observation that this flow type is the most common for microemulsions [20, 27].

Figure 4c represents how η of the two investigated systems, W/SL-IPA/IPM and W/SM-IPA/IPM, was affected by gradual addition of water. The η values of all microemulsions at SCoS/O ratio of 9:1 were in range between 3 and 110 mPas. In concordance with conductance results, η values strongly depended on Φ_w . It seems that changes in η with increasing Φ_w can be ascribed to the structural changes and therefore the occurrence of microemulsion phase inversion. In principle, three slopes were observed in viscosity plots, and these results correlate well with features of conductivity curves, implying three different microstructures regimes. Although microemulsions are macroscopically homogenous, they are structured microscopically, and all of the structural changes that occur in the isotropic region develop continuously during progressive dilution with water [42]. It is notable that the obtained trend of viscosity profiles is far different from the bell-shaped viscosity curve commonly seen in similar studies [e.g., 44]. Nevertheless, such behavior correlates well with the viscosity plots of the systems: water + propylene glycol/sucrose laurate/benzaldehyde + ethanol and water/sucrose laurate + propylene glycol/oleyl lactate [27, 32]. Both systems contained SE as a surfactant, implying that this behavior may be a consequence of the properties of surfactant on its own.

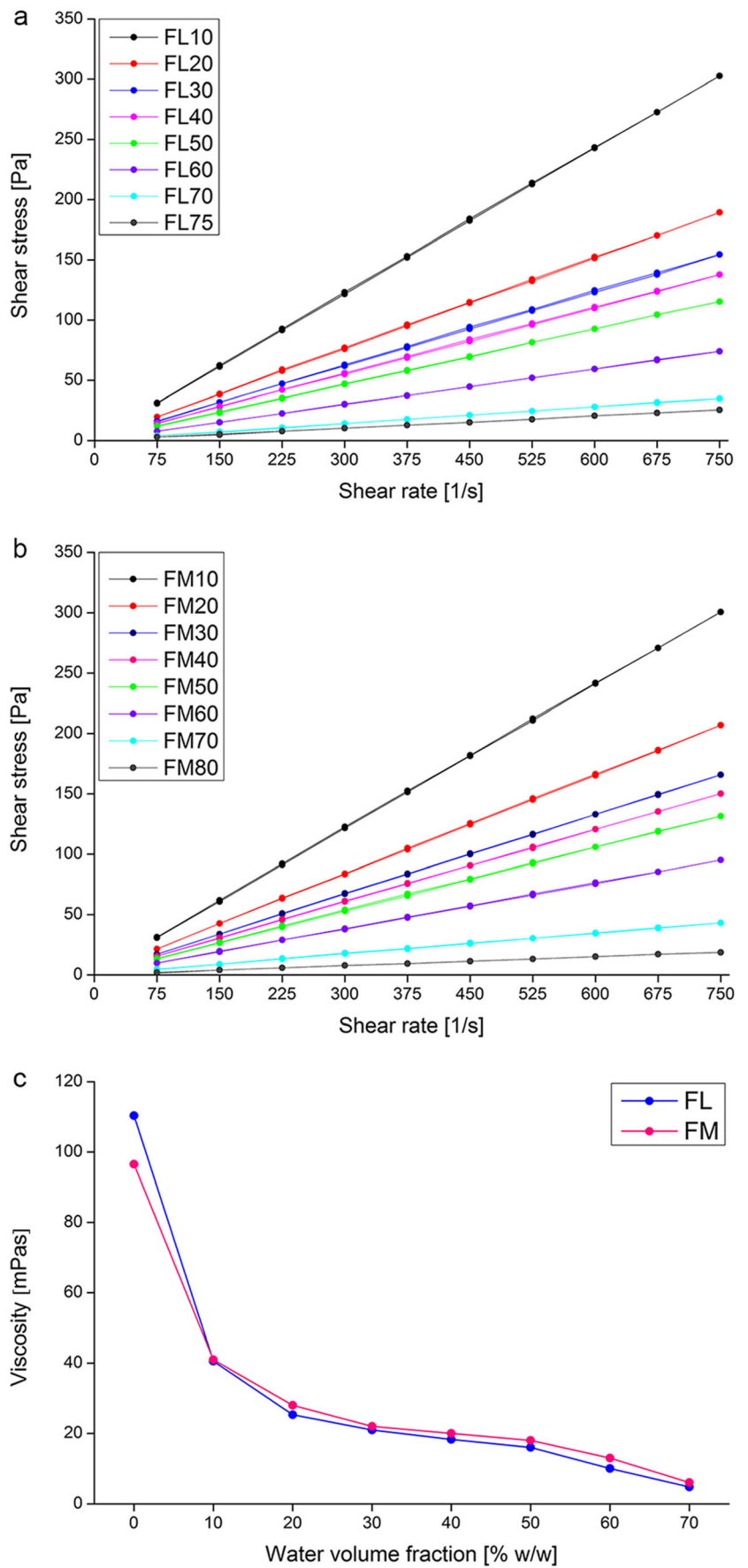
The high viscosity values of systems without water (FL0 and FM0) were most probably due to the strong intermicellar interaction. Depending on the composition, η values decreased as the added Φ_w increased. These results were not consistent with the observation of η values increases with the water content increase or turning the system from W/O to oil-in-water (O/W) type [9]. In fact, our results demonstrated a sharp decrease in η (from 110 and 97 mPas to 40 mPas for SL and SM, respectively) with the addition of water, perhaps because dilution of continuous phase gave rise to reduction of micellar aggregation phenomena. These results are in accordance with earlier observation by Fisher et al. [27]. A slight viscosity decrease in the Φ_w range between 20 and 60 % (w/w) suggests structure transition from oil-continuous, via intermediate bicontinuous, to water-continuous system. The phenomenon of η reduction with water content increase from 20 to

about 60 % (w/w) seems to be attributable to a shift of the surfactant molecules from the bulk to the interface, to cover water and oil in a bicontinuous microemulsion as proposed by Fanun [45]. The relatively low viscosity values suggested the lack of anisometric aggregates, which is in line with the lack of anisotropy under polarization light. However, further reduction in η at higher water content may be attributable to a gradual disintegration of the bicontinuous structure. Further, as the added Φ_w was more than 60 % (w/w), the η continued to decrease, possibly due to lower viscosity of the continuous phase and progressive water dilution, which caused reduction in the inter-droplet interactions [20, 46]. Thus, the relatively low values of viscosity with Φ_w above 60 % (w/w) may be correlated with the occurrence of individual spherical droplets of the inner oil phase dispersed in water continuous medium.

DSC—thermal investigations

DSC cooling curves, presented in Fig. 5, highly supported the results of conductivity and viscosity measurements. Ultra-purified water, used in this study, showed a sharp, exothermic peak at -6.92 °C (onset -9.52 °C). Since samples FL0 and FM0 do not contain water, it is clear that the respective peaks at -28.03 and -26.72 °C do not represent water in any state. This conclusion was also confirmed by the evaluation of thermal behavior of surfactant blends (data not shown), and thus, it is reasonable to suppose that small exothermic peaks (between -30 and -15 °C) of samples FL0-10 and FM0-10 represented solidification of IPM or its impurities. In accordance with conductivity and viscosity data, it is evident that water molecules are bound or interact strongly with either sucrose head groups of SEs or with IPA. Both interactions alter thermodynamic properties of water, moving its freezing point to temperatures below the limit of detection set in our study. In fact, at water concentrations below 20 % (w/w), no freezing peak of water molecules was observed, demonstrating presence of a nonfreezable aqueous phase in W/O microemulsions. Nevertheless, in curves of both samples with 20 % (w/w) water, structure inversion may be deduced from appearance of a new broad peak. Samples FL20-60 and FM20-50 have manifested a peak in the range -60 to -30 °C, indicating bound or interfacial water in these systems. A relatively low water freezing temperature can be attributed to the strong water–surfactant and water–IPA interactions, presumably via hydrogen bonds, based on their polar nature and the presence of hydroxyl groups in their structure [28, 47]. With higher content of water, the peak area increased and the peak moved toward higher temperatures, indicating weakening of interactions, as well as water drift to the outer phase. In fact, with gradual addition of water, concentration of IPA and SE decreased; thus, water molecules became progressively less bound, as it could be seen by increasing freezing temperature as well as enthalpy of freezing (Table 2).

Fig. 4 **a** The flow curves of W/SL-IPA/IPM microemulsions at SCoS/O ratio 9:1. **b** The flow curves of W/SM-IPA/IPM microemulsions at SCoS/O ratio 9:1. **c** Apparent viscosity as a function of the water volume fraction for W/SL-IPA/IPM (FL) and W/SM-IPA/IPM (FM) microemulsions at SCoS/O ratio 9:1



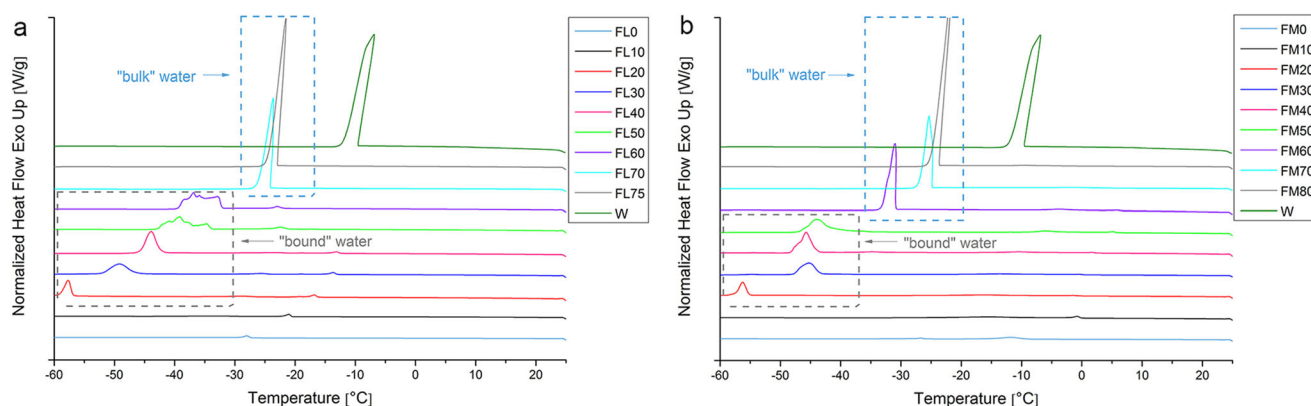


Fig. 5 **a** DSC cooling curves of water (*W*) and W/SL-IPA/IPM microemulsions at SCoS/O ratio 9:1. **b** DSC cooling curves of water (*W*) and W/SM-IPA/IPM microemulsions at SCoS/O ratio 9:1

With further addition of water (equal or more than 70 and 60 % (*w/w*), in case of SL and SM, respectively), surfactant head groups and IPA became fully hydrated and a distinctive change in patterns of DSC curves was observed. In line with the viscosity and conductivity data, the detected large sharp peak may be attributed to freezing of bulk water. The addition of water may have facilitated migration of alcohol out of the interface to the continuous phase. IPA, along with surfactant head groups, binds some of the water molecules causing slight deviation in freezing behavior of water molecules. Therefore, the peak of bulk water, loosely bound to the alcohol or surfactants head group, suggests changes in microemulsion structure from bicontinuous to O/W. In accordance with these observations, the lack of exothermic peak of IPM at water content above 60 % (*w/w*) suggests an oil drift to internal phase. Finally, the exothermic peak of bulk water became even more pronounced as the water content further increased. Notably, the sharp water peak has appeared earlier in the case of SM. This can be attributed to the more hydrophilic nature of SL, due to its shorter chain length and stronger water binding to the sucrose head group. Based on this, head groups of SL are more exposed to water and therefore have affected more strongly the water molecules. Consequently, in the SL-based system, bulk water was firstly detected at 70 % (*w/w*), whereas

in SM-based system, the first detection was at Φ_w values of 60 % (*w/w*).

AFM as a direct measurement technique

In order to choose the optimal sample preparation steps, we compared the AFM images of the microemulsions after vacuum drying and after drying in desiccator. As no significant differences between the two sets of images were apparent (data not shown), the sample preparation set on its own does not introduce any artifacts, and we opted to perform the study with use of desiccator drying.

The atomic force micrographs depicted in Fig. 6 represent the structures observed for droplet and bicontinuous microemulsions which contain SL as surfactant. In case of the sample FL10, the isolated globular structures with a diameter less than 100 nm represent preliminary evidence for the existence of water droplets in the oil-rich region. It can be seen from Fig. 6 that FL40 microemulsion sample is undeniably different from structures noted with FL10 and FL70 droplet microemulsions. This micrograph also showed the characteristic, mutually intertwined domains of oil and water with fluctuating curvature associated with inner structuration of bicontinuous microemulsions, which

Table 2 Thermodynamic parameters of water peak in W/SL-IPA/IPM and W/SM-IPA/IPM microemulsions at SCoS/O ratio 9:1

	Sucrose laurate-based microemulsions								
	FL0	FL10	FL20	FL30	FL40	FL50	FL60	FL70	FL75
Enthalpy [J/g]	–	–	52.94	83.35	126.41	151.83	212.10	297.34	360.02
Onset [°C]	–	–	–56.9	–45.46	–42.35	–37.61	–35.13	–24.07	–22.93
Peak [°C]	–	–	–57.65	–49.01	–43.94	–39.21	–36.82	–23.62	–21.48
	Sucrose myristate-based microemulsions								
	FM0	FM10	FM20	FM30	FM40	FM50	FM60	FM70	FM80
Enthalpy [J/g]	–	–	51.95	88.11	128.89	146.60	238.66	271.86	373.93
Onset [°C]	–	–	–55.17	–43.39	–43.99	–41.28	–30.85	–24.78	–23.65
Peak [°C]	–	–	–56.24	–45.23	–45.75	–43.97	–30.95	–25.34	–21.40

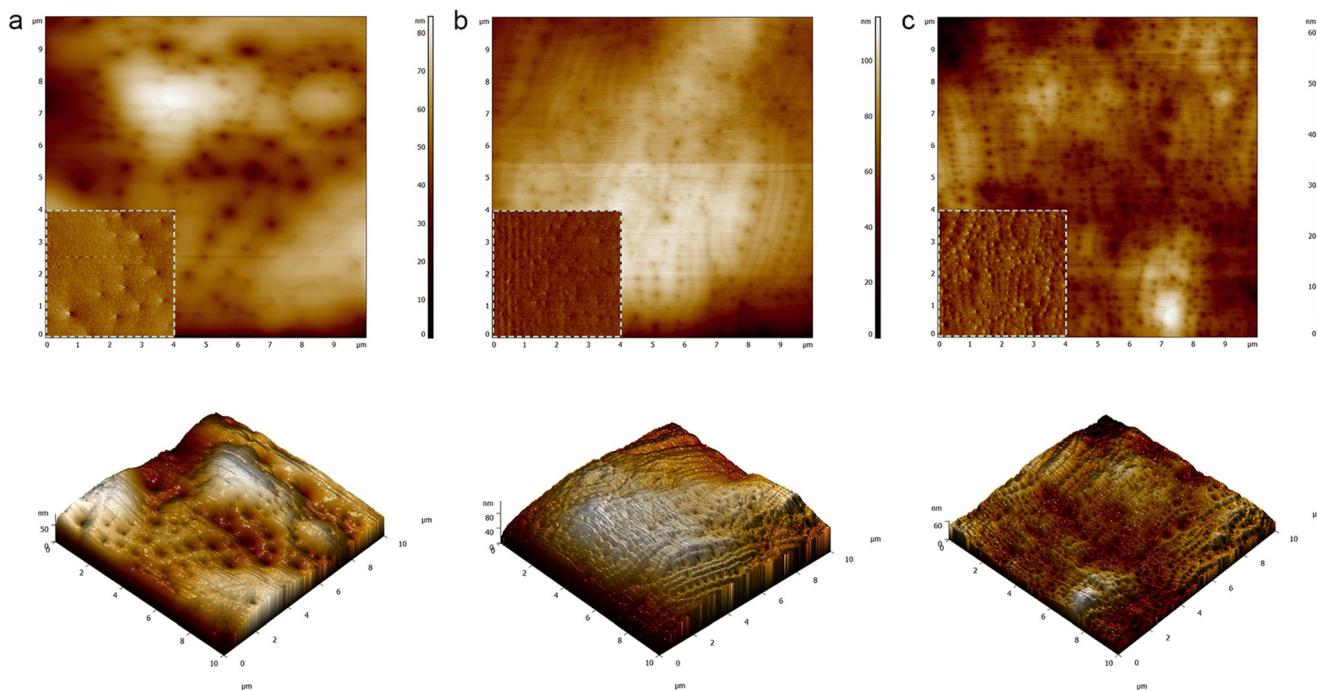


Fig. 6 AFM images showing the structures of droplet and bicontinuous microemulsions. 2D and 3D topography images of the samples: **a** FL10, **b** FL40, and **c** FL70, are shown with smaller 2D error signal images inserted into 2D topography images

was already suggested by conductivity, rheology, and DSC data. The droplets seem to have tendency to aggregate and form elongated polygon-type structures. In fact, the microemulsion structure shown in Fig. 6b can be interpreted as water aggregates in coexistence with bicontinuous domains. After percolation threshold, droplets' interface became fluid enough for their collision, and thereafter, the formation of clusters and water channels ensued. Thus, AFM images confirmed the structural transition from discrete water aggregates to a connected water network, giving a proof for the existence of a bicontinuous structure in the sample FL40. Moreover, the notable geometrical disorder distinguished them from the lamellar liquid crystals, as geometrically ordered structures with higher viscosity and pseudo-plastic flow behavior [10]. These observations are in line with the lack of anisotropy when samples were analyzed under polarization light.

Oil droplets in the sample FL70 with Φ_w of 70 % (w/w) were bigger in comparison with water droplets of FL10 (78.5 vs. 39.8 nm), as measured by cross-sectional image analysis shown in Fig. 7. In fact, a larger droplet size of O/W microemulsions may be attributed to the IPM localization and its amphiphilic nature, which are responsible for repulsion between hydrophilic moieties of surfactants, as shown by Bardhan et al. [48]. The presented AFM images highly support results obtained from indirect measurements techniques, and all these data are concordant in pointing to the structural system transit from oil-continuous via bicontinuous to water-continuous.

Solubilization of aceclofenac as pharmaceutical active ingredient

The complex and diverse microstructure of microemulsions and different aqueous volume fractions offered an advantage of having various formulations for aceclofenac solubilization. In accordance with the observed phase behavior of SEs, solubilization capacity of aceclofenac was evaluated along the characterized water dilution line. It was noticed that the loading capacity for aceclofenac decreased as dilution progressed. Interestingly, the observed loading capacity was similar irrespective of the used surfactant. SL- and SM-based microemulsions with equal content of water (35 % (w/w)) were chosen as the most appropriate for complete solubilization of aceclofenac, as further increase in water content was accompanied by the formation of drug precipitate. This behavior may be linked to the aceclofenac structure, which contains both apolar large domain as well as carboxyl group as a small polar part of the molecule, as shown in Table 3. With its lipophilic and hydrophilic domains (mesogenic structure), the solubilized aceclofenac itself could act as cosurfactant, raising the probability of incorporation into the surfactant interfacial film and not remaining solely in the oil phase (as parent molecule) nor in the water phase (as ionized molecule). In order to confirm this assumption and to elucidate possible aceclofenac distribution, a solubilization capacity evaluation was performed, in parallel with solubility study in liquid excipients. Table 3 shows that solubility of aceclofenac was very

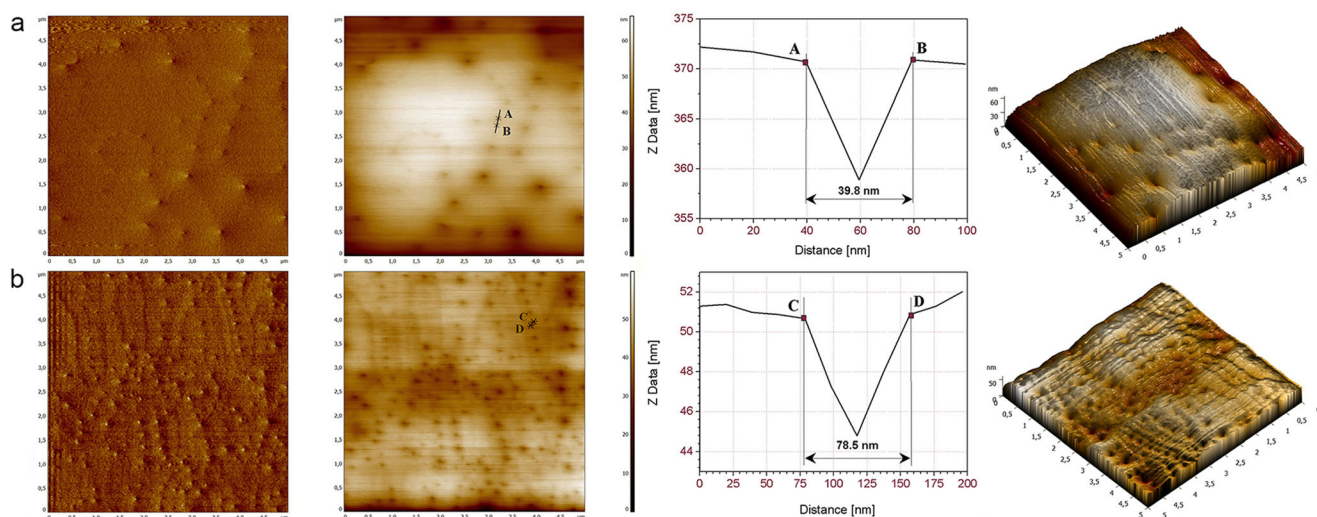


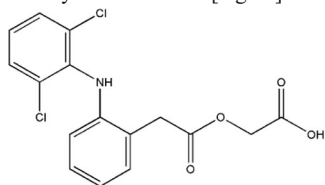
Fig. 7 Cross-sectional analysis of AFM images as a tool used for the determination of droplet size of the samples: **a** FL10 and **b** FL70

similar in both surfactant blends, as well as in pure IPA. Solubility study in pure surfactants (SL and SM) was not performed due to their solid state. Despite high aceclofenac solubility in IPA (Table 3) and having in mind that a crucial prerequisite for the vehicles' clinical use is their biocompatibility, we considered SE-based microemulsions as optimal vehicles for aceclofenac dermal delivery, as their topical application allows high flux rates of drug due to high solubilization capacity in combination with an established permeation enhancing effect. Counterintuitively, aceclofenac solubility in IPM was almost 14 times lower than in surfactant blends and 74.16 times higher than in water. Thus, taking into account high surfactant concentration, and considering the solubility of aceclofenac in components, it could be assumed that aceclofenac mostly locates at the oil–water interface. These observations were also supported with theoretical background that hydrophobic drugs are predominantly incorporated into the oil phase, whereas hydrophilic substances are primarily dissolved in the polar water phase. Accordingly, it is reasonable to suppose that major fraction of a drug with mesogenic structure should be located at the

oil–water interface [49, 50]. With increasing water volume fraction, the surfactant film at the interface available for drug solubilization decreases, far different from bicontinuous microemulsion structure proposed to be optimal for aceclofenac incorporation. Highly dynamic character of bicontinuous microemulsion may enhance transport of a drug through the skin. Additionally, very low interfacial tension of bicontinuous microemulsion could improve wetting of the stratum corneum which may also facilitate drug transport [51]. Nevertheless, the solubility potential of microemulsion systems may be an important factor for aceclofenac release, as drug release and consequently drug delivery toward deeper parts of the skin, or even to the blood, are related to the concentration gradient according to the Fick law of diffusion. In this regard, high solubilization capacity of such systems is expected to increase the concentration gradient, which further improves drug release and penetration. Due to the expected benefits of its bicontinuous structure after topical application, aceclofenac-loaded microemulsions with SL and SM as surfactants with Φ_w of 35 % (w/w) will be subject of further investigations.

Table 3 Solubility of aceclofenac in selected components of microemulsions [mg/ml]±SD

	W	IPA	IPM	SL/IPA	SM/IPA
Solubility of aceclofenac [mg/ml]	0.06±0.01	56.40±0.89	4.46±0.06	59.16±1.22	52.49±1.03



Conclusion

It can be concluded that tail length of SEs substantially affects not only the amount of solubilized water and consequently the area of microemulsion region but also the structure of microemulsion. The conductivity results revealed the presence of a percolation threshold and, in accordance with viscosity and DSC data, provided convincing evidence that the microemulsion system undergoes a structural inversion. The W/O microemulsions, O/W microemulsions, and a region between them, corresponding to bicontinuous microemulsions, have been proposed using indirect measurement techniques, which has been proved by images obtained with AFM technique. The type of microemulsion strongly influenced the extent of aceclofenac solubilized, and it can be assumed that aceclofenac-loaded bicontinuous microemulsions with 35 % of water (*w/w*) may enhance the transport of the drug through the skin. Finally, mixture experiment approach appeared to be convenient in detection of boundaries of microemulsion area, and it may be recommended as an effective tool to reduce experimental load.

Acknowledgments The authors would like to acknowledge the financial support from the Ministry of Education, Science and Technological Development, Republic of Serbia, through Project TR34031 and TR32008. The authors are grateful to Mitsubishi-Kagaku Foods Corporation for supplying sucrose esters.

References

- Klang V, Matsko N, Zimmermann AM, Vojnikovic E, Valenta C (2010) Enhancement of stability and skin permeation by sucrose stearate and cyclodextrins in progesterone nanoemulsions. *Int J Pharm* 393:152–160
- Ullrich S, Metz H, Mäder K (2008) Sucrose ester nanodispersions: microviscosity and viscoelastic properties. *Eur J Pharm Biopharm* 70:550–555
- Schwarz JC, Klang V, Hoppel M, Mahrhauser D, Valenta C (2012) Natural microemulsions: formulation design and skin interaction. *Eur J Pharm Biopharm* 81:557–562
- Kürti L, Veszélka S, Bocsik A, Dung NT, Ozsvári B, Puskás LG, Kittel A, Szabó-Révész P, Deli MA (2012) The effect of sucrose esters on a culture model of the nasal barrier. *Toxicol In Vitro* 26:445–454
- Szűts A, Szabó-Révész P (2012) Sucrose esters as natural surfactants in drug delivery systems—a mini-review. *Int J Pharm* 433:1–9
- Sahle FF, Metz H, Wohrlab J, Neubert RH (2013) Lecithin-based microemulsions for targeted delivery of ceramide AP into the stratum corneum: formulation, characterizations, and in vitro release and penetration studies. *Pharm Res* 30:538–551
- Tirnaksiz F, Kayış A, Çelebi N, Adışen E, Erel A (2012) Preparation and evaluation of topical microemulsion system containing metronidazole for remission in Rosacea. *Chem Pharm Bull* 60:583–592
- Bolzinger-Thevenin MA, Grossiord JL, Poelman MC (1999) Characterization of a sucrose ester microemulsion by freeze fracture electron micrograph and small angle neutron scattering experiments. *Langmuir* 15:2307–2315
- Boonme P, Krauel K, Graf A, Rades T, Junyaprasert VB (2006) Characterization of microemulsion structures in the pseudoternary phase diagram of isopropyl palmitate/water/Brij 97:1-butanol. *AAPS PharmSciTech* 7:E45
- Alany RG, Tucker IG, Davies NM, Rades T (2001) Characterizing colloidal structures of pseudoternary phase diagrams formed by oil/water/amphiphile systems. *Drug Dev Ind Pharm* 27:31–38
- Klang V, Valenta C, Matsko NB (2013) Electron microscopy of pharmaceutical systems. *Micron* 44:45–74
- Krauel K, Girvan L, Hook S, Rades T (2007) Characterisation of colloidal drug delivery systems from the naked eye to Cryo-FESEM. *Micron* 38:796–803
- Kang BK, Chon SK, Kim SH, Jeong SY, Kim MS, Cho SH, Lee HB, Khang G (2004) Controlled release of paclitaxel from microemulsion containing PLGA and evaluation of anti-tumor activity in vitro and in vivo. *Int J Pharm* 286:147–156
- Fanun M, Papadimitriou V, Xenakis A (2011) Characterization of cephalixin loaded nonionic microemulsions. *J Colloid Interface Sci* 361:115–121
- Gaur PK, Mishra S, Aeri V (2014) Formulation and evaluation of Guggul lipid nanovesicles for transdermal delivery of aceclofenac. *Sci World J* 2014:534210
- Lee J, Lee Y, Kim J, Yoon M, Choi YW (2005) Formulation of microemulsion systems for transdermal delivery of aceclofenac. *Arch Pharm Res* 28:1097–1102
- Shakeel F, Baboota S, Ahuja A, All J, Shafiq S (2008) Skin permeation mechanism of aceclofenac using novel nanoemulsion formulation. *Pharmazie* 63:580–584
- Fanun M (2009) Oil type effect on diclofenac solubilization in mixed nonionic surfactants microemulsions. *Colloid Surf A: Physicochem Eng Aspects* 343:75–82
- Podlogar F, Gašperlin M, Tomšič M, Jamnik A, Bešter Rogač M (2004) Structural characterisation of water-Tween 40/Inwitor 308-isopropyl myristate microemulsions using different experimental methods. *Int J Pharm* 276:115–128
- Santana RC, Fasolin LH, da Cunha RL (2012) Effects of a cosurfactant on the shear-dependent structures of systems composed of bio-compatible ingredients. *Colloid Surf A: Physicochem Eng Aspects* 398:54–63
- Wan T, Hu ZW, Ma XL, Yao J, Lu K (2008) Synthesis of silane monomer-modified styrene-acrylate microemulsion coatings by photopolymerization. *Prog Organ Coat* 62:219–225
- Akalin Ö, Akay KU, Sennaroglu B, Tez M (2010) Optimization of chemical admixture for concrete on mortar performance tests using mixture experiments. *Chemom Intell Lab Syst* 104:233–242
- Design-Expert 7.0.0 User's Guide, (2005) Stat-Ease, Inc., Minneapolis, MN, USA
- Jeirani Z, Jan BM, Ali BS, Noor IM, Hwa SC, Saphanuchart W (2012) The optimal mixture design of experiments: alternative method in optimizing the aqueous phase composition of a microemulsion. *Chemom Intell Lab Syst* 112:1–7
- Furlanetto S, Cirri M, Piepel G, Mennini N, Mura P (2011) Mixture experiment methods in the development and optimization of microemulsion formulations. *J Pharm Biomed Anal* 55:610–617
- Barot BS, Parejiya PB, Patel HK, Gohel MC, Shelat PK (2012) Microemulsion-based gel of terbinafine for the treatment of onychomycosis: optimization of formulation using D-optimal design. *AAPS PharmSciTech* 13:184–192
- Fisher S, Wachtel EJ, Aserin A, Garti N (2013) Solubilization of simvastatin and phytosterols in a dilutable microemulsion system. *Colloid Surf B Biointerfaces* 107:35–42
- Garti N, Aserin A, Tiunova I, Fanun M (2000) A DSC study of water behavior in water-in-oil microemulsions stabilized by sucrose esters and butanol. *Colloid Surf A: Physicochem Eng Aspects* 170:1–18

29. Bardhan S, Kundu K, Saha SK, Paul BK (2013) Physicochemical studies of mixed surfactant microemulsions with isopropyl myristate as oil. *J Colloid Interface Sci* 402:180–189
30. Mehta SK, Kaur G, Mutneja R, Bhasin KK (2009) Solubilization, microstructure, and thermodynamics of fully dilutable U-type Brij microemulsion. *J Colloid Interface Sci* 338:542–549
31. Fanun M (2008) Surfactant chain length effect on the structural parameters of nonionic microemulsions. *J Disp Sci Techn* 29:289–296
32. Fanun M (2008) Phase behavior, transport, diffusion and structural parameters of nonionic surfactants microemulsions. *J Mol Liq* 139: 14–22
33. Alany RG, Agatonovic-Kustrin S, Rades T, Tucker IG (1999) Use of artificial neural networks to predict quaternary phase systems from limited experimental data. *J Pharm Biomed Anal* 19:443–452
34. Djekic L, Ibric S, Primorac M (2008) The application of artificial neural networks in the prediction of microemulsion phase boundaries in PEG-8 caprylic/capric glycerides based systems. *Int J Pharm* 361: 41–46
35. Richardson CJ, Mbanefo A, Aboofazeli R, Lawrence MJ, Barlow DJ (1997) Prediction of phase behavior in microemulsion systems using artificial neural networks. *J Colloid Interface Sci* 187:296–303
36. Miguélez-Morán A-M (2009) Roller compaction of pharmaceutical ingredients: on the understanding of the compaction and the use of knowledge based applications in the formulation of tablets. Dissertation, University of Heidelberg, Germany
37. Wesolowski M, Suchacz B (2012) Artificial neural networks: theoretical background and pharmaceutical applications: a review. *J AOAC Int* 95:652–668
38. Mehta SK, Bala K (1995) Volumetric and transport properties in microemulsions and the point of view of percolation theory. *Phys Rev E Stat Phys Plasmas Fluids Relat Interdiscip Topics* 51:5732–5737
39. Borkovec M, Eicke HF, Hammerich H, Das Gupta B (1988) Two percolation processes in microemulsions. *J Phys Chem* 92:206–211
40. Chakraborty I, Moulik SP (2005) Physicochemical studies on microemulsions 9. Conductance percolation of AOT-derived W/O microemulsion with aliphatic and aromatic hydrocarbon oils. *J Colloid Interface Sci* 289:530–541
41. Jeirani Z, Jan BM, Ali BS, Noor IM, Hwa SC, Saphanuchart W (2012) Prediction of water percolation threshold of a microemulsion using electrical conductivity measurements and design of experiments. *Ind Eng Chem Res* 51:10147–10155
42. Mehta SK, Kaur G (2011) Microemulsions: thermodynamic and dynamic properties. In: Tadashi M (ed) *Thermodynamics*. In Tech, Rijeka, pp 381–406
43. Podlogar F, Bešter Rogač M, Gašperlin M (2005) The effect of internal structure of selected water-Tween 40-Imwitor 308-IPM microemulsions on ketoprofene release. *Int J Pharm* 302:68–77
44. Mitra RK, Paul BK (2005) Physicochemical investigations of microemulsification of eucalyptus oil and water using mixed surfactants (AOT+Brij-35) and butanol. *J Colloid Interface Sci* 283:565–577
45. Fanun M (2007) Conductivity, viscosity, NMR and diclofenac solubilization capacity studies of mixed nonionic surfactants microemulsions. *J Mol Liq* 135:5–13
46. Fanun M (2010) Solubilization of celecoxib in microemulsions based on mixed nonionic surfactants and peppermint oil. *J Disp Sci Techn* 31:1140–1149
47. Yaghmur A, Aserin A, Tiunova I, Garti N (2002) Sub-zero temperature behaviour of non-ionic microemulsions in the presence of propylene glycol by DSC. *J Thermal Anal Calorim* 69:163–177
48. Bardhan S, Kundu K, Paul BK, Saha SK (2013) Interfacial composition and characterization of a quaternary water-in-oil mixed surfactant (cationic of different alkyl chain lengths + polyoxyethylene type nonionic) microemulsions in absence and presence of inorganic salts. *Colloid Surf A: Physicochem Eng Aspects* 433:219–229
49. Djekić L, Primorac M, Filipić S, Agbaba D (2012) Investigation of surfactant/cosurfactant synergism impact on ibuprofen solubilization capacity and drug release characteristics of nonionic microemulsions. *Int J Pharm* 433:25–33
50. Lawrence MJ, Rees GD (2012) Microemulsion-based media as novel drug delivery systems. *Adv Drug Deliv Rev* 64:175–193
51. Bolzinger MA, Carduner T, Poelman MC (1998) Bicontinuous sucrose ester microemulsion: a new vehicle for topical delivery of niflumic acid. *I J Pharm* 176:39–45